

Probing the structure of nanodiscs using surface induced dissociation

Sophie R. Harvey^{a*}, Zachary L. VanAernum^{a*}, Marius M. Kostelic^b, Michael T. Marty^b, Vicki H. Wysocki^a

Methods

Sample preparation

1,2-Dimyristoyl-*sn*-glycero-3-phosphocholine (DMPC) and 1,2-dimyristoyl-*sn*-glycero-3-phospho-(1'-rac-glycerol) (DMPG) lipids were purchased from Avanti Polar Lipids. Ammonium acetate, Amberlite XAD-2, and sodium cholate were purchased from Sigma-Aldrich. Gramicidin A was purchased from Alfa Aesar. Membrane scaffold protein MSP1D1(-) was expressed in *E. coli* and purified by immobilized metal affinity chromatography (IMAC), as previously described.^{1, 2} Nanodiscs were assembled using a previous established protocol.^{1, 2} Briefly, DMPC and DMPG lipid stocks in chloroform were dried under nitrogen and then resolubilized in sodium cholate. MSP1D1(-) was then added to the lipid solution, and the detergent was removed by addition of Amberlite XAD-2 hydrophobic beads. Nanodiscs were purified into 200 mM ammonium acetate at pH 6.8 using a Superose 6 Increase 10/300 column (GE Healthcare).³

For gramicidin nanodiscs, gramicidin A was dissolved in methanol and added directly to the preformed nanodiscs, as previously reported.⁴ In brief, 19 μL of 2.5 μM nanodisc was mixed with 3 μL of 0.2 mM peptide and 1.5 μL of 0.4 M imidazole. For nanodiscs without gramicidin incorporated, 19 μL of 2.5 μM nanodisc was mixed with 3 μL of methanol and 1.5 μL of 0.4 M imidazole to keep solution conditions consistent between experiments.

Native MS methods

All experiments were conducted on a Thermo Q Exactive Ultra High Mass Range (UHMR) MS (Bremen, Germany), which has been modified to include SID, as described below. Mass calibration is performed using a 2 mg/mL solution of Csl in 50:50 water:isopropanol, following the manufacturers protocol covering the m/z range 386.7-11298.7. All samples were ionized *via* static nanospray ionization using in-house pulled borosilicate capillaries with the electrospray voltage applied to a platinum wire in contact with the solution. An in-source collision induced dissociation voltage of 50 - 60 V and source temperature of 200 °C were applied to aid desolvation. RF amplitudes of 550-700 V were applied to the injection flatapole, 940 V to the bent flatapole and 900 V to the HCD cell. A trap gas pressure setting of 7 (arb.) was applied and a maximum injection time of 200–400 ms was used for all experiments. A wide isolation window around the nanodisc peaks was applied to remove interference from free lipid and low mass lipid clusters; the width and position of the isolation window was optimized for each sample and was typically 5000–8000 m/z wide centered around 7000–10000 m/z . The resolution, as defined at m/z 400, was set to 12,500. For MS and CID experiments, the SID device was tuned to allow transfer of ions through the device without hitting the surface, and for SID experiments, the device was tuned such that the ions were directed towards and collide against the surface. For CID and SID experiments, the collision voltage was typically ramped from 0–225 V. All data were deconvolved over the m/z range 4,000–25,000 using UniDec and MetaUniDec. UniDec uses a Bayesian framework to separate mass and charge dimensions, and is well suited to handling overlapping charge state distributions present in nanodisc spectra because it can factor in information from both adjacent charge states as well as know mass differences, in this case due to different numbers of lipids per complex. Full details on the deconvolution algorithm and its application to nanodiscs have been previously described.^{5, 6} UniDec was downloaded from GitHub

(<https://github.com/michaelmarty/UniDec/releases>). Data were deconvolved considering charge states 1–25 and a mass range of 20,000–200,000 Da. The deconvolved mass was sampled every 10 Da. A known mass difference of 678 or 667 Da were used to aid deconvolution for DMPC and DMPG nanodiscs respectively. The automatic peak width tool was used, and a charge smooth width of -1 and mass smooth width of -2 were used. Macromolecular mass defect analysis was used to determine the number of membrane scaffold belt proteins present after SID, and to determine the number of peptides in the nanodisc pre and post SID. In the mass defect analysis the measured mass is divided by a reference mass (in this case the lipid mass) and then the remainder of the division is plotted, normalized between 0 and 1.^{4,7}

Modification of the UHMR for SID

The Thermo Q Exactive UHMR was modified to incorporate an SID device, similar to the previous modifications performed on an Exactive Plus EMR modified with a quadrupole.⁸ The SID cell was similar to the previously reported design, with modified PEEK spacers and additional PEEK standoffs on the entrance lens which increased ease and reproducibility in mounting and alignment. The SID cell was installed in place of the octupole between the selection quadrupole and the C-trap. Voltages were supplied to the SID cell and C-trap offset *via* external dc power supplies (Ardara Technologies, Ardara, PA) and controlled through the accompanying Tempus Tune software (Ardara Technologies, Ardara, PA). The surface was prepared as follows; a 17-mm × 13-mm × 0.5-mm gold surface slide, 1,000 Å of Au on 50 Å of Ti on glass (EMF Corp.), was cleaned for 15 min in a UV cleaner (Model 135500; Boekel Scientific). The cleaned surface was then incubated in ~3 mL of 1 mM solution of perfluorothiol (FC₁₂) in ethanol in the dark.⁹ Following incubation, the surface was cleaned by sonicating in ~3 mL of ethanol for 1 min; this cleaning process was repeated six times with fresh aliquots of ethanol.⁹

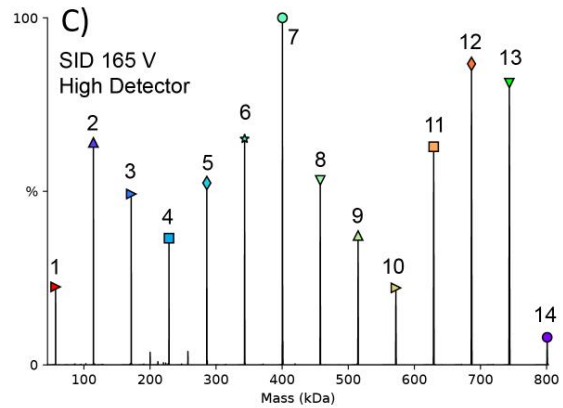
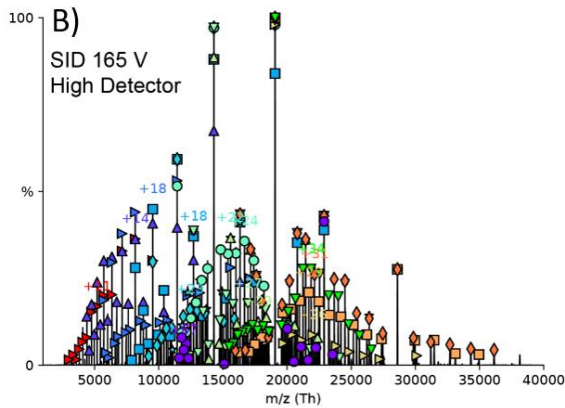
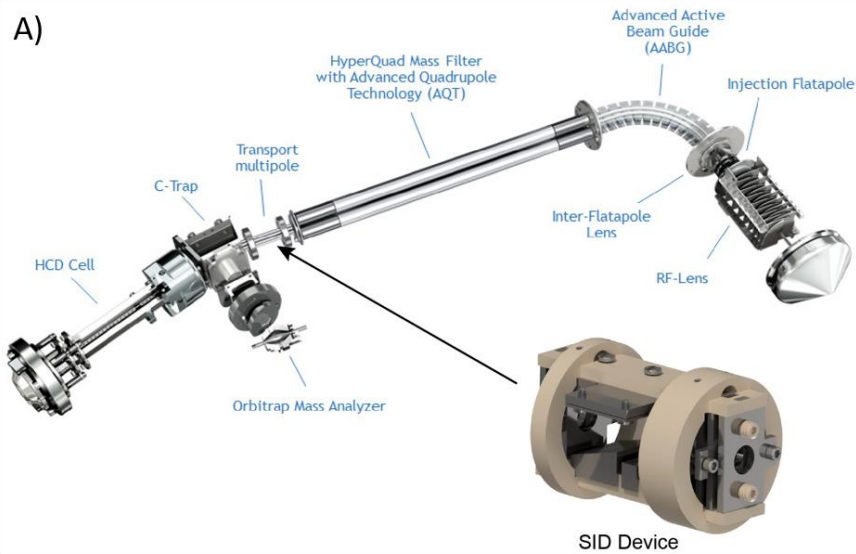


Figure S1: A) Schematic of the Q Exactive UHMR with the transport multipole replaced with an SID device. Instrument schematic from Thermo Scientific. B) Representative 7-ring-on-7-ring GroEL 14-mer (charge states 74+ to 65+) dissociated by 165 V of SID shown as a mass spectrum and C) deconvoluted mass spectrum. The most abundant charge state of each species is labeled in panel B, and each oligomeric state is labeled with the number of subunits in panel C. Data were deconvolved using UniDec.

Implementation of temperature recording in the UHMR Nanospray Flex source

A temperature and humidity sensor was built and added to the Nanospray Flex ion source. A DHT22 combination temperature and humidity sensor was mounted inside of the clear acrylic glass portion of the Nanospray Flex source, approximately 5 cm from the nanospray emitter. The DHT22 sensor was connected to an Arduino Uno using a LEMO push pull connector to allow for disconnection of the sensor cable when the source is removed. The sensor was read every 30 seconds by the Arduino Uno and written over a serial port and recorded in a spreadsheet on the instrument control computer.

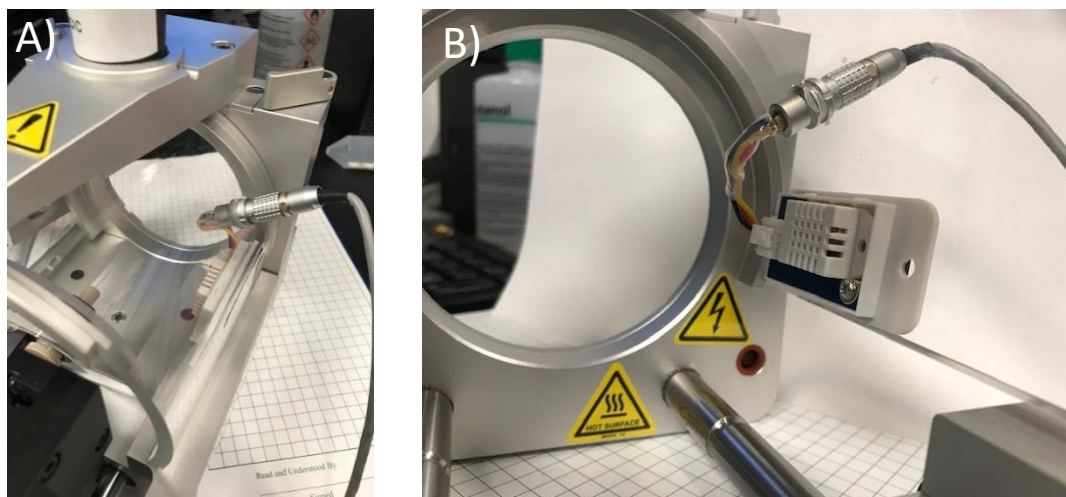


Figure S2: Temperature and humidity sensor installed in the Nanospray Flex source showing the A) outside view of the source and B) the inside view of source.

Additional figures and discussion

DMPC nanodiscs

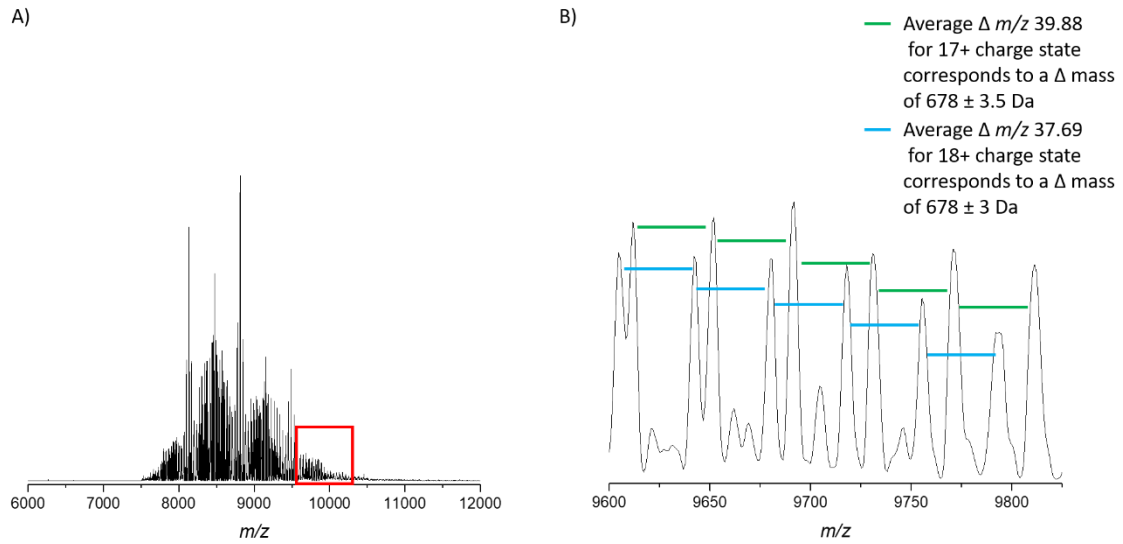


Figure S3: DMPC Nanodisc native mass spectrum acquired on a Thermo Q Exactive UHMR, with 60 V in-source CID and HCD 0 V. The unlabeled y-axis represents relative intensity. A) full MS over m/z range 6000-1200, B) zoom in of m/z 9600-9825, showing overlapping distributions from nanodiscs containing different numbers of lipids at the 17+ or 18+ charge state. Mass differences corresponding to a single DMPC lipid can be manually identified.

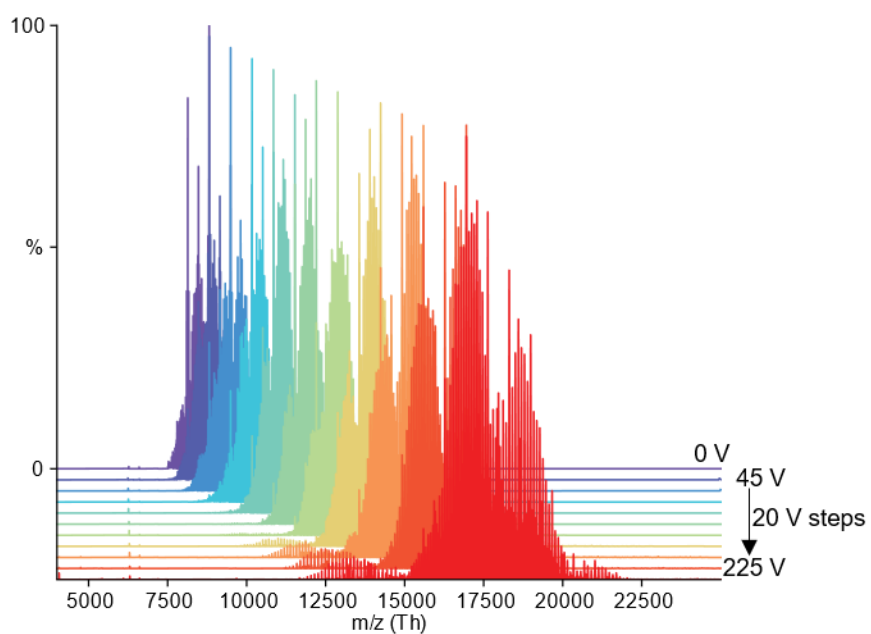


Figure S4: Waterfall plot showing dissociation of one replicate of DMPC nanodiscs as a function of HCD voltage, from HCD 0–225 V, with an additional 60 V in-source CID. Nanodisc signal moves to higher m/z due to loss of charged lipid clusters (note that the y-axis represents m/z , not mass; the corresponding plot with mass as the x-axis is Figure 1).

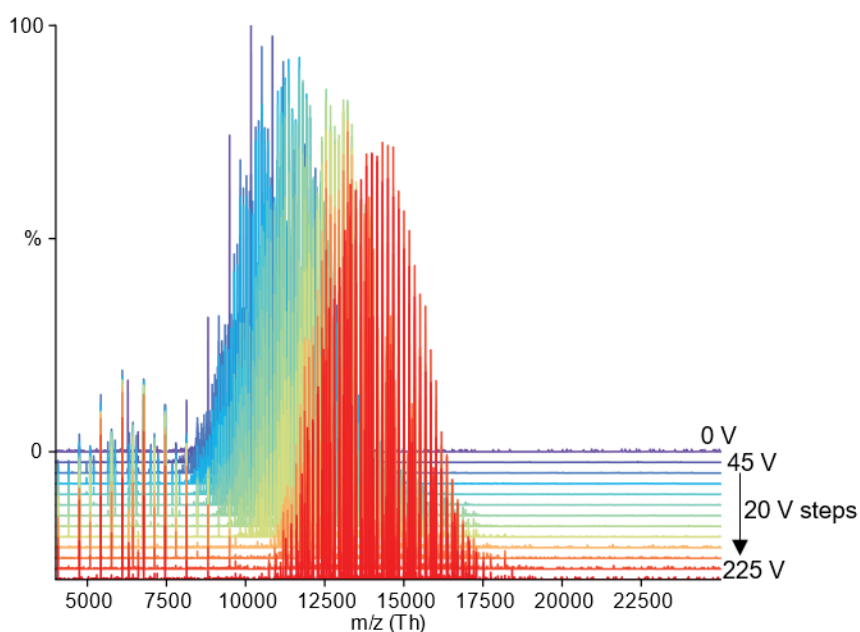


Figure S5: Waterfall plot showing dissociation of one replicate of DMPC nanodiscs as a function of SID voltage, from SID 0–225 V, with an additional 60 V in-source CID. In comparison to Figure S4 a decreased shift in m/z is observed here indicative of the more symmetric dissociation.

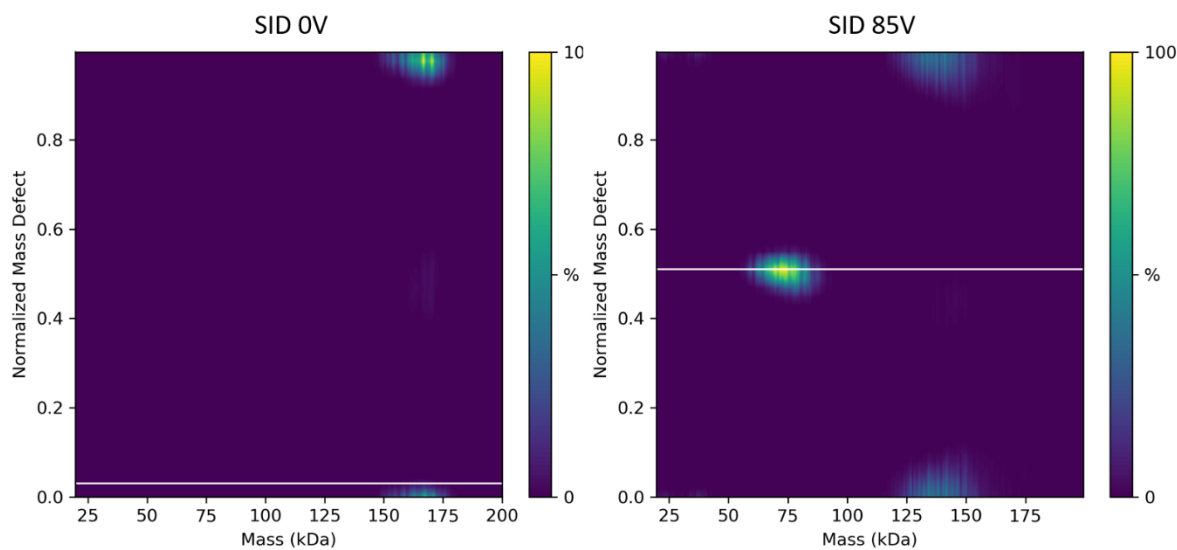


Figure S6: Macromolecular mass defect plots of the A) the intact DMPC nanodisc (SID 0 V), where the horizontal line represents the theoretical mass defect for two membrane scaffold belt proteins and B) the DMPC nanodisc after dissociation to half nanodisc (SID 85V), where the horizontal line represents the theoretical mass defect for one membrane scaffold belt protein. Most of the intensity for A is wrapped to the top of the display (the measured mass defect is slightly lower than the calculated).

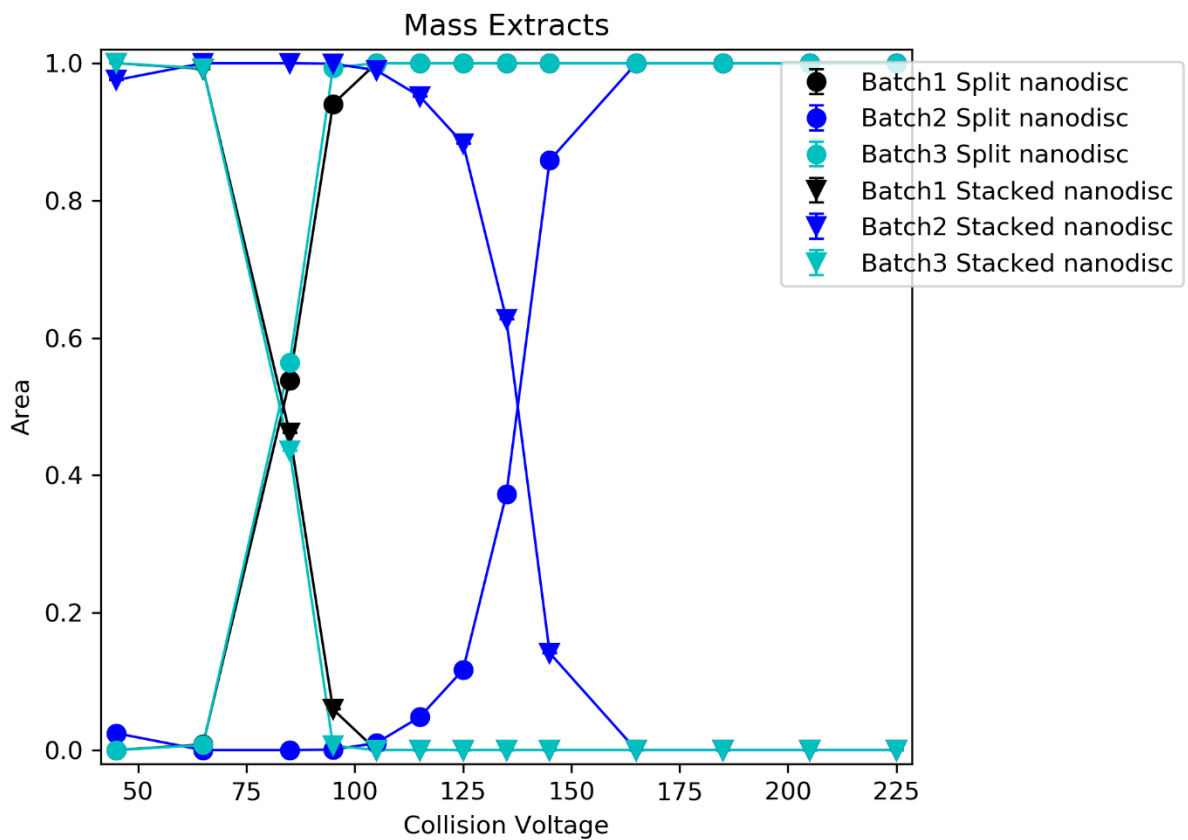


Figure S7: Stacked and split nanodisc abundance as a function of SID collision voltage for three different preparations of DMPC nanodiscs. Data were processed using MetaUniDec, and the area for each set of peaks was extracted using UltraMeta with average masses of 142,380 and 66,110 Da for stacked and split nanodisc respectively and a broad mass window of 20,000 Da.

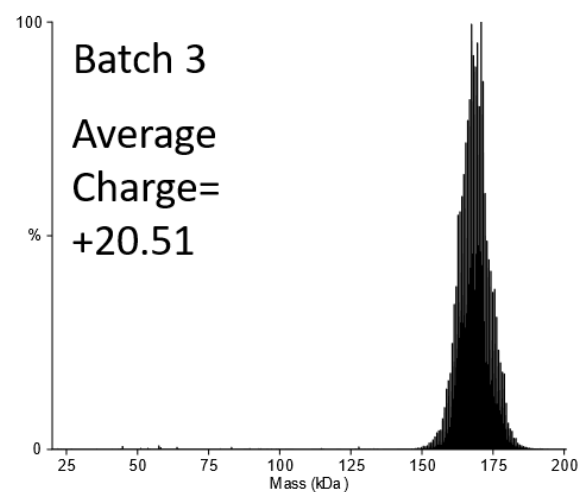
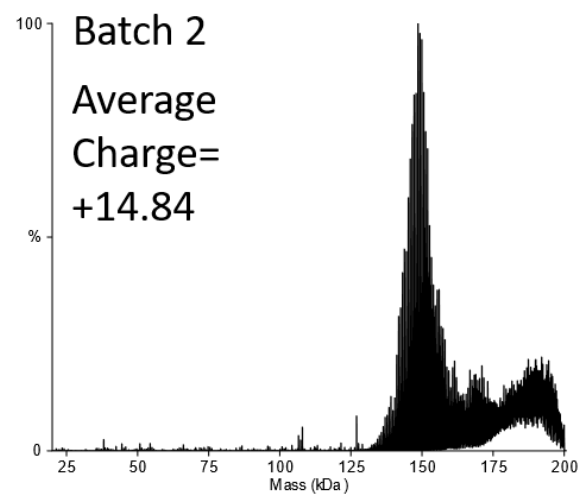
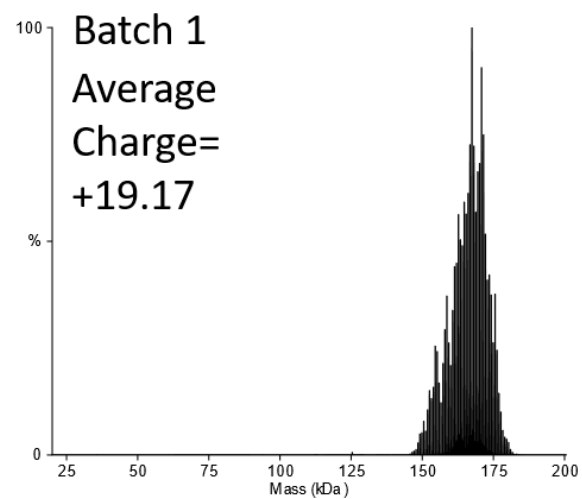


Figure S8: Deconvolved mass spectra for the three different batches of DMPC nanodiscs, spectra acquired with an in-source CID of 50-60 V and HCD 0 V. Average charge state is noted for each replicate. Deconvolution and average charge state analysis was performed using UniDec.⁵

Variability in energy required to dissociate 50% of nanodisc

Given the differences observed between the batches (Figure S7), and to assess the variability between the same batch, the voltage ramp experiments were repeated performing technical replicates on the same batch of sample. Three same-day replicates were performed, changing the nESI needle between each replicate. For the three replicates of the same batch we still observe a slight shift in the fragmentation onset (Figure S9); as these were all replicates of the same batch, this rules out batch-to-batch variability as the major factor contributing to variable fragmentation onset. We did observe slight shifts in mass and average charge state, replicate to replicate (Figure S10), and attribute that to the different nESI needles used for each replicate. However, these shifts are relatively minor compared to the shifts in onset energy; correcting for max charge in MetaUniDec⁶ did not reduce the variability significantly (Figure S11).

The phase transition temperature of DMPC is around room temperature (T_m 24 °C)¹⁰ and could affect the stability of the bilayer, which could pose a challenge in studying these nanodiscs at room temperature. Therefore, we considered whether fluctuations in the temperature could also be contributing to this variability. Before performing the same batch replicates, a temperature sensor was installed in the Nanospray Flex ion source to record the temperature inside of the source every 30 seconds (see methods for more information). Our measurements showed that the ambient source temperature was on average 27.5 ± 0.8 °C for these experiments. Given the small difference between our experimental temperature and the T_m , it is possible that conformational change as a result of phase transition is playing a role in the onset energy variability.

We believe, however, that an additional source of variability is due to lipids from the nanodisc sticking to the SID surface upon collision and changing the properties of the surface, an effect we have not previously observed when studying protein complexes, peptides, or membrane proteins solubilized in detergent. Previous reports for intentionally-modified surfaces have shown that the surface material and uniformity can affect the SID products formed.^{11, 12} This suggests that for future studies changing (or perhaps heating) the surface after nanodisc experiments may be necessary; future experiments will seek to further characterize this. To determine if the variability within a set of nanodisc experiments could be reduced by intentionally coating the surface with lipids *in vacuo*, we performed SID at 105 V on a DMPC nanodisc for over 14 hours and then repeated the energy ramp experiments on the same batch of samples used for the technical replicate experiments. In this case, we still observed variability in the onset of fragmentation (Figure S12). In these experiments, half nanodiscs are consistently observed as the major product, following some lipid loss, hence as the major products are the same between trials, discussion in this study focuses on the products as opposed to onset energies.

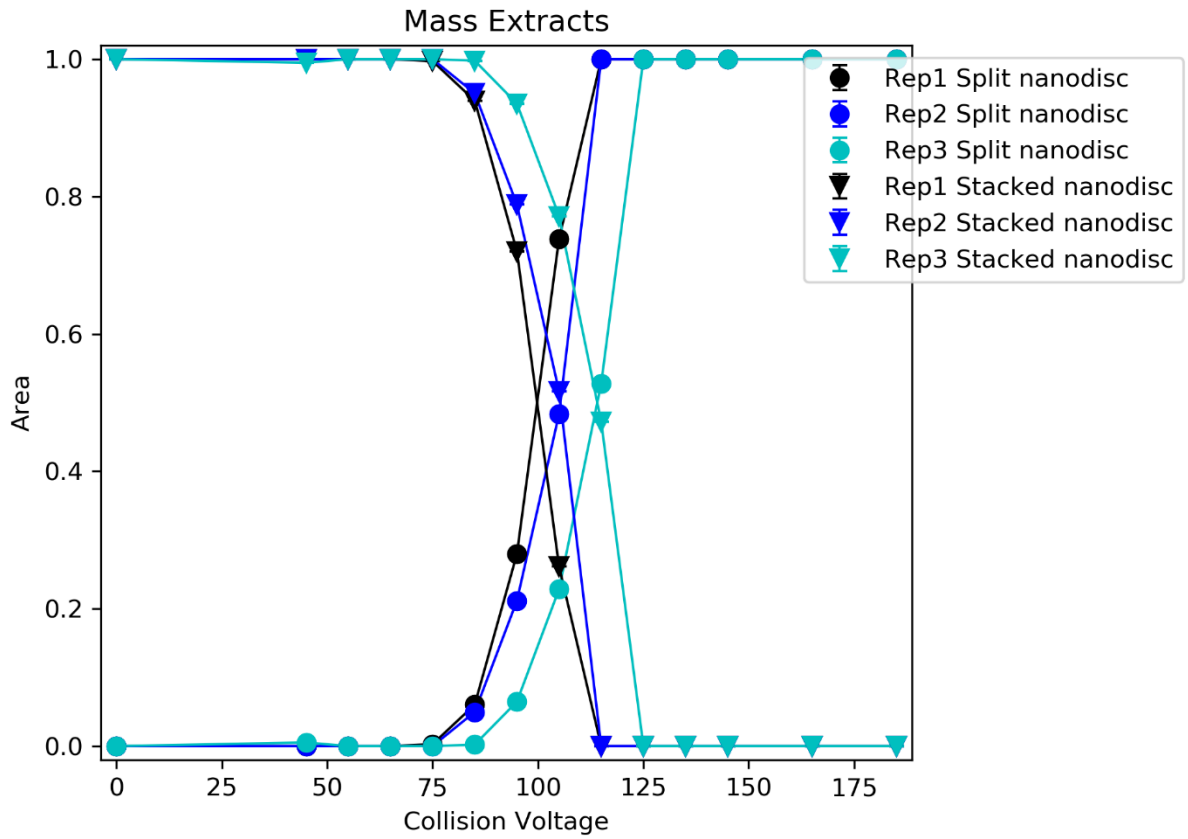


Figure S9: Stacked and split nanodisc abundance as a function of SID collision voltage for three same-day replicates of the same preparation of DMPC nanodiscs. Data was deconvolved using MetaUniDec, and the area of each set of peaks was extracted using UltraMeta with average masses of 135,600 and 59,330 Da for stacked and split nanodiscs, respectively, and a broad mass window of 20,000 Da.

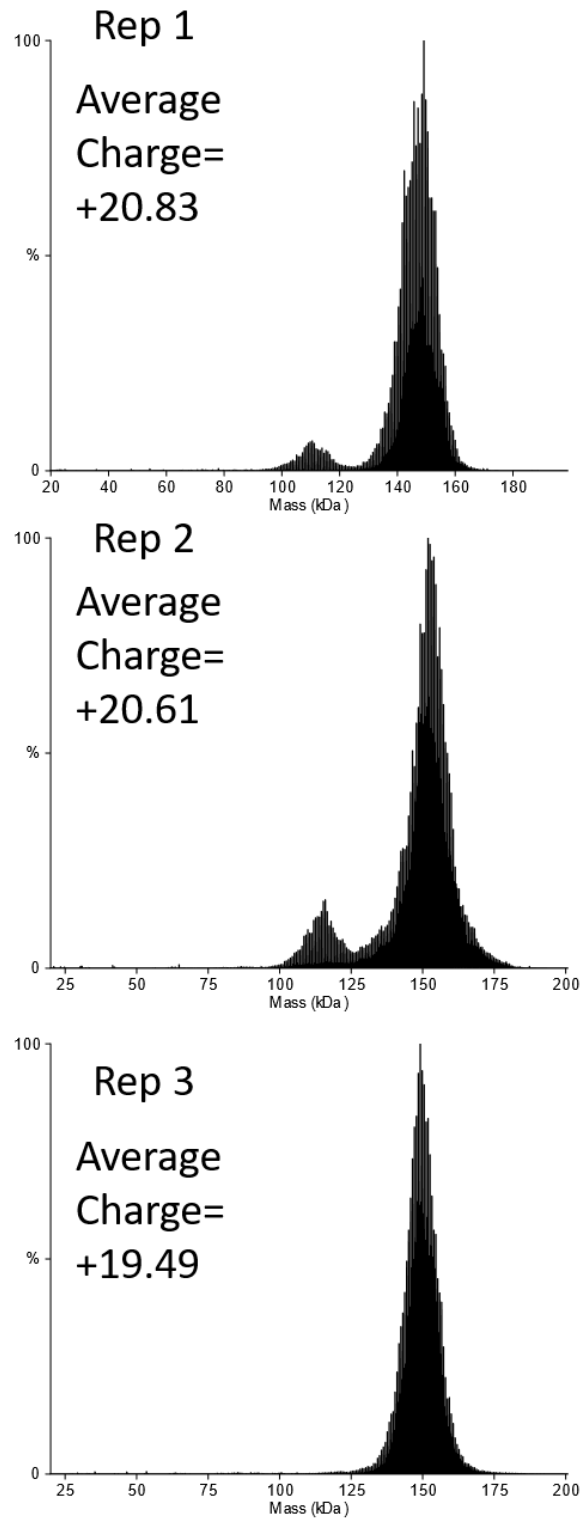


Figure S10: Deconvolved mass spectra for the three technical replicates of the same batch of DMPC nanodiscs. Average charge state is noted for each replicate. Deconvolution and average mass analysis was performed using UniDec.⁵

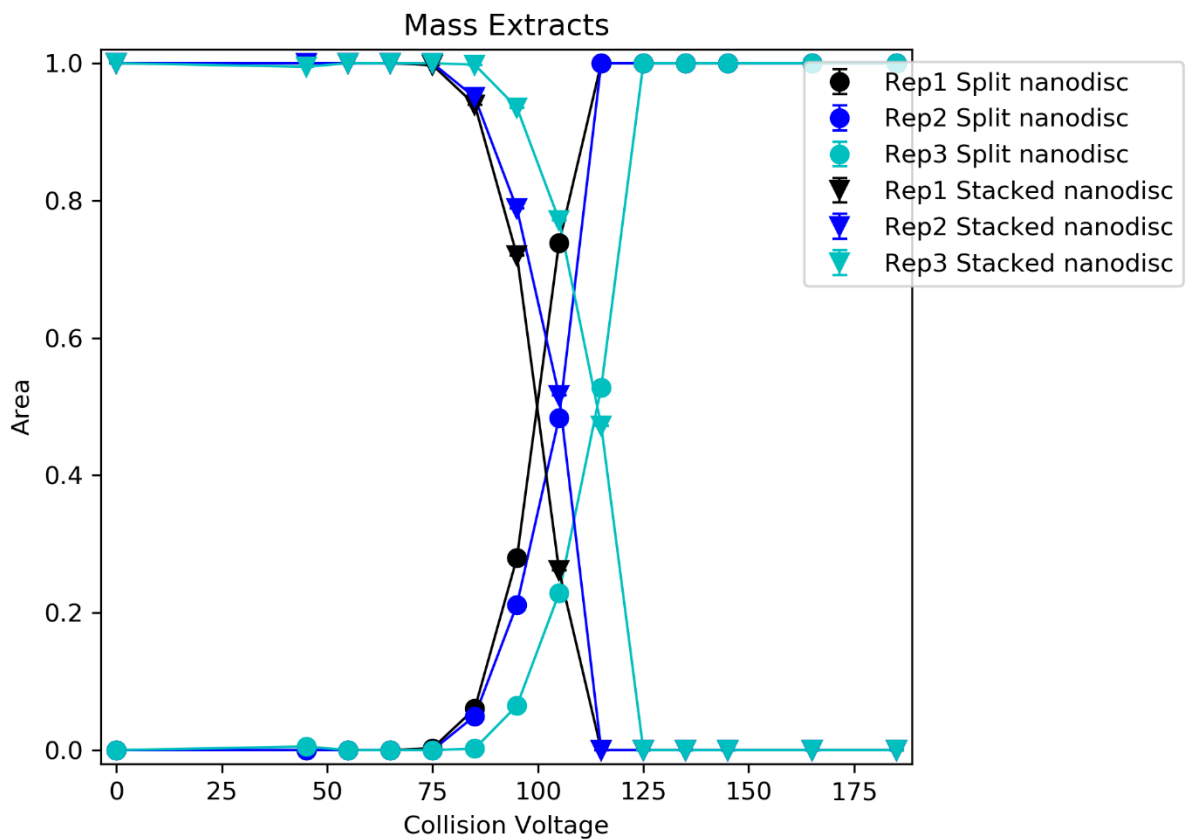


Figure S11: Stacked and split nanodisc abundance, as a function of SID collision voltage for three replicates of the same preparation of DMPC nanodiscs. Corrected for Max charge. Data processed using MetaUniDec and the area of each set of peaks was extracted using UltraMeta with average masses of 135,600 and 59,330 Da for stacked and split nanodiscs, respectively, and a broad mass window of 20,000 Da.

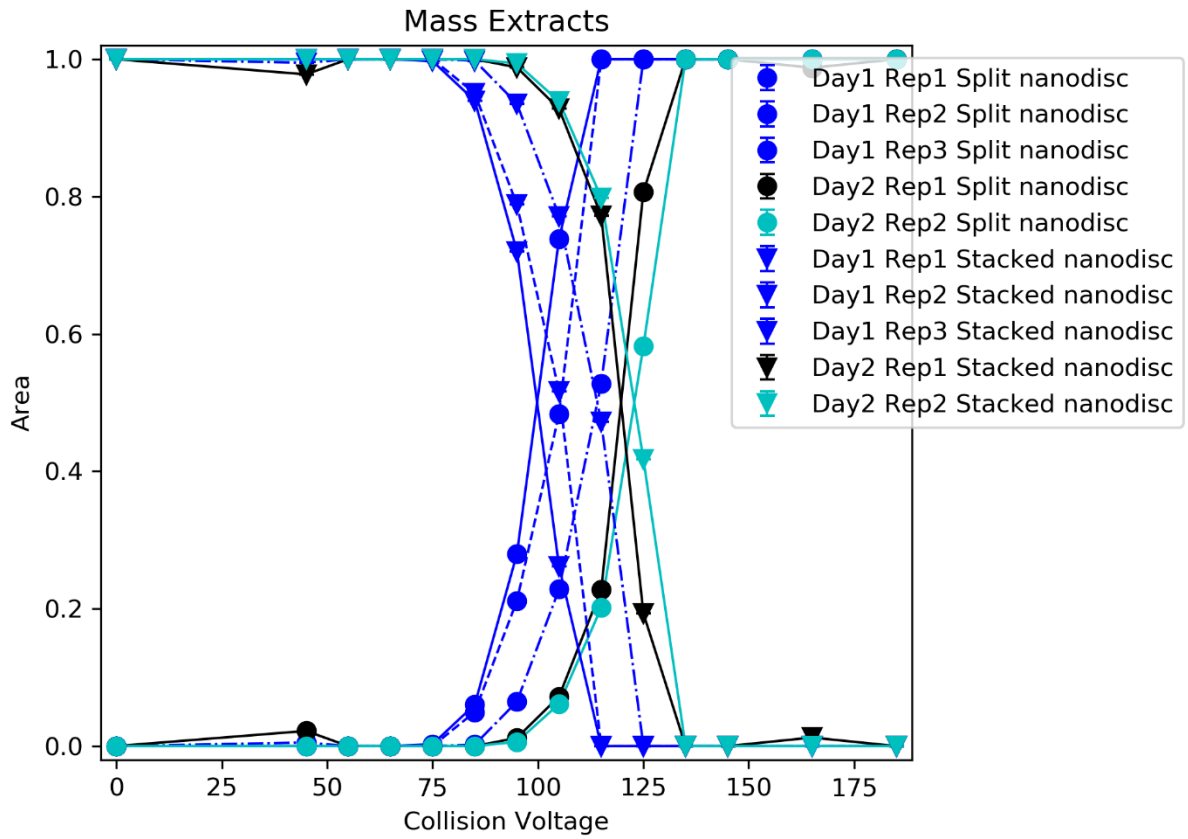


Figure S12: Stacked and split nanodisc abundance as a function of SID collision voltage for replicates of the same preparation of DMPC nanodiscs, before (data shown in S11 and here in blue, Day 1) and after (black and teal, Day 2) overnight collision with lipids. Data processed using MetaUniDec, and the area of each set of peaks was extracted using UltraMeta with average masses of 135,600 and 59,330 Da for stacked and split nanodiscs, respectively, and a broad mass window of 20,000 Da.

DMPG nanodiscs

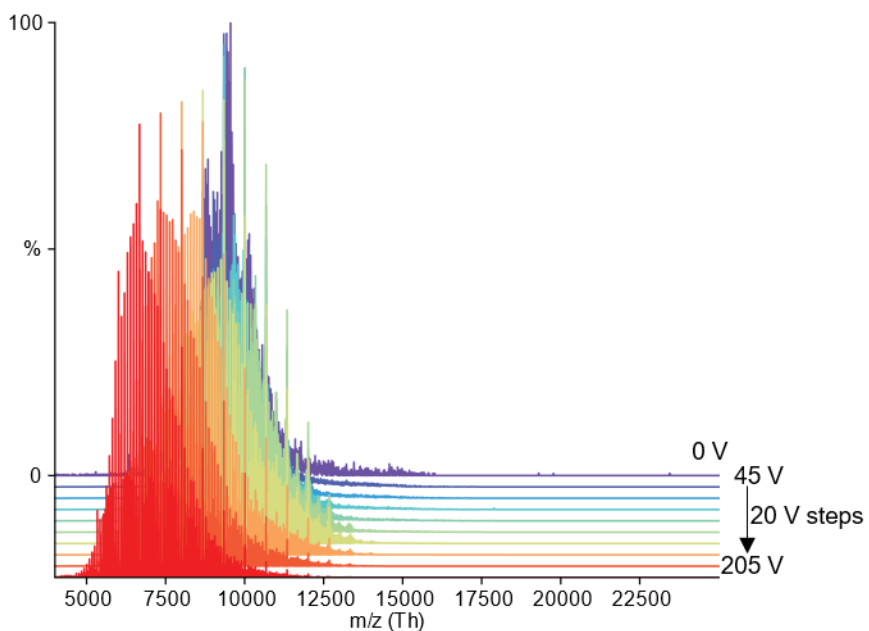


Figure S13: Waterfall plot showing dissociation of DMPG nanodiscs as a function of HCD voltage, over the voltage range 0–205 V, with an additional 50 V in-source CID.

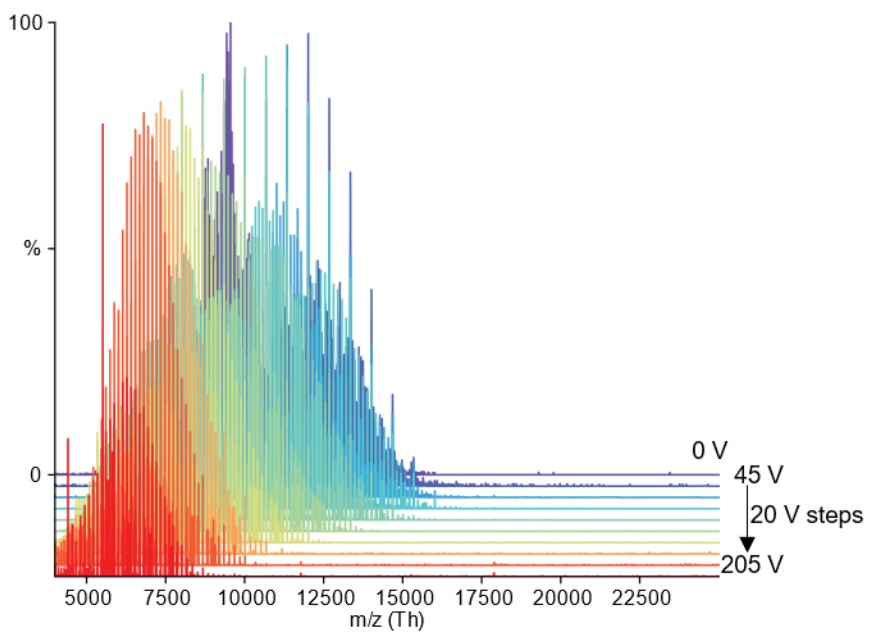


Figure S14: Waterfall plot showing dissociation of DMPG nanodiscs as a function of SID voltage, over the voltage range 0–205 V, with an additional 50 V in-source CID.

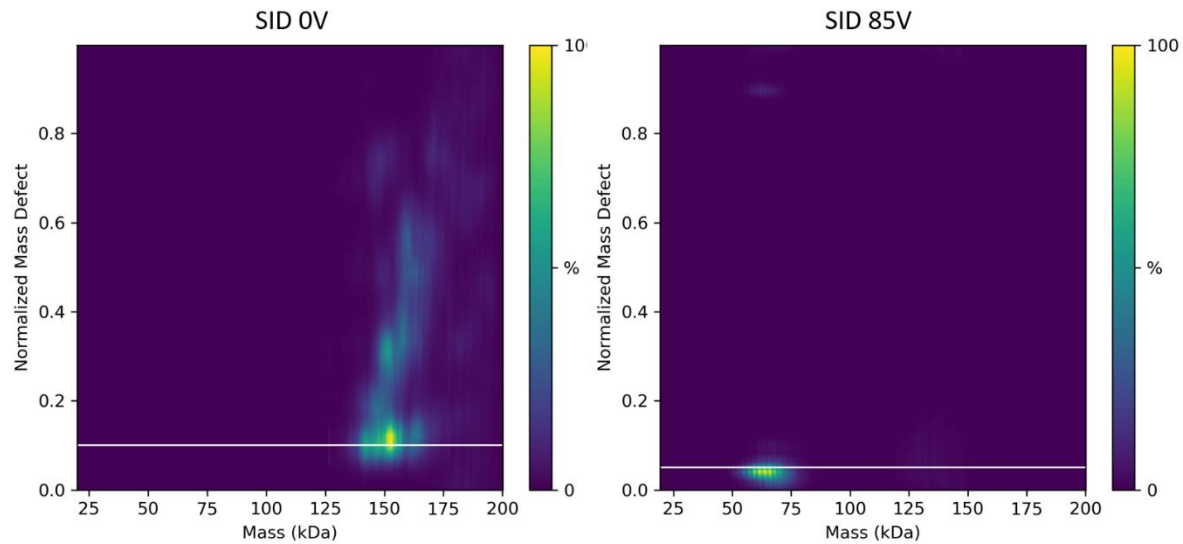


Figure S15: Macromolecular mass defect plots of the A) the intact DMPG nanodisc (SID 0 V), where the horizontal line represents the theoretical mass defect for two membrane scaffold belt proteins and B) the DMPG nanodisc after dissociation to half nanodisc (SID 85V), where the horizontal line represents the theoretical mass defect for one membrane scaffold belt protein.

50:50 DMPC:DMPG nanodiscs

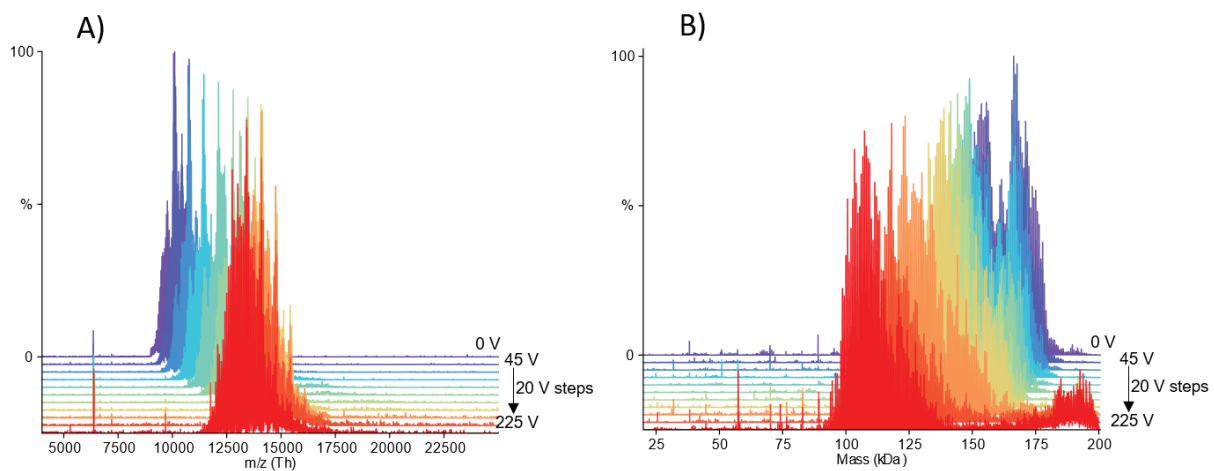


Figure S16: Waterfall plot showing dissociation of DMPC:DMPG nanodiscs as a function of HCD voltage, from 0–225 V, with an additional 50 V in-source CID. MS/MS m/z data shown in (A) and deconvolved (mass) data shown in (B).

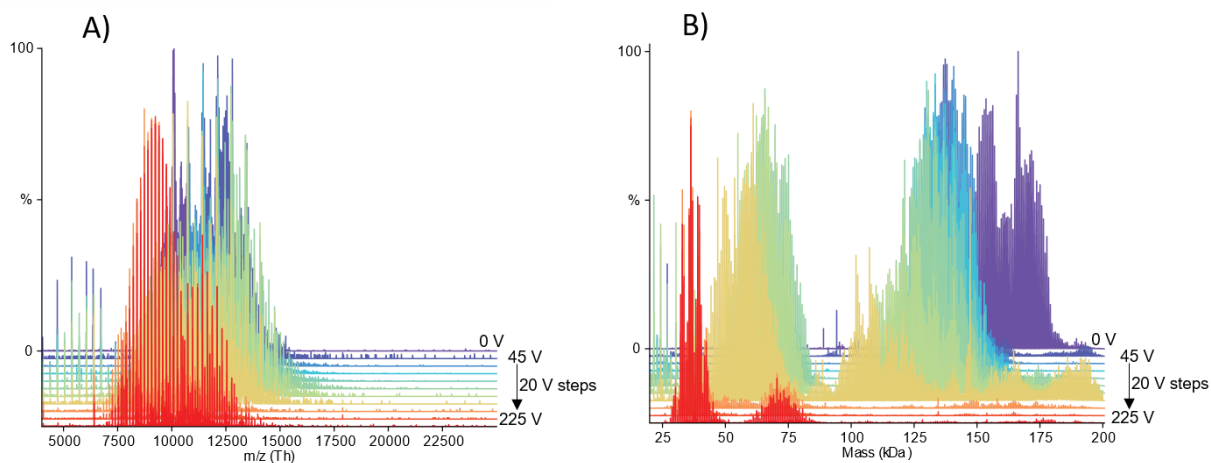


Figure S17: Waterfall plot showing dissociation of DMPC:DMPG nanodiscs as a function of SID voltage, from 0–225 V, with an additional 50 V in-source CID. MS/MS m/z data shown in (A) and deconvolved (mass) data shown in (B).

Gramicidin containing nanodiscs

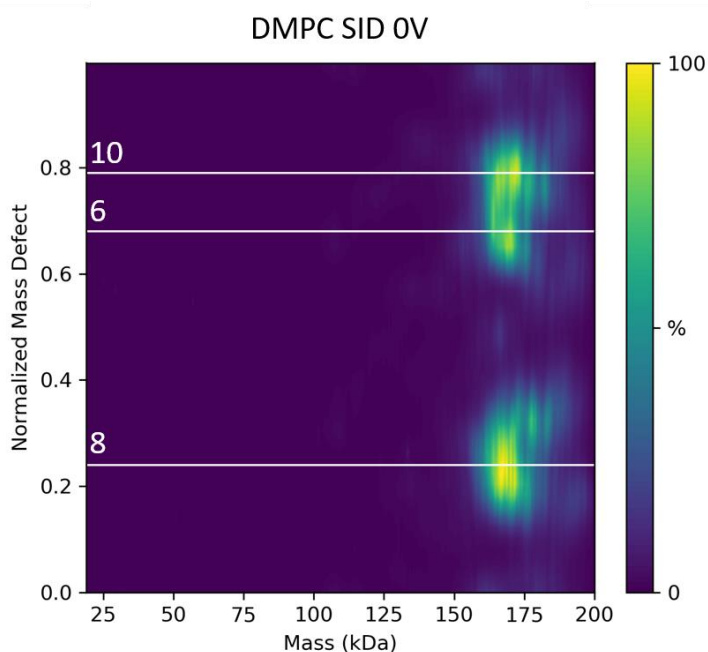


Figure S18: Macromolecular mass defect plot for DMPC nanodiscs containing gramicidin. Horizontal lines represent the theoretical mass defect for two membrane scaffold belt proteins and 6, 8, or 10 gramicidin peptides and are labelled for the number of gramicidin peptides. Note, given the higher background for the DMPG nanodisc (see Figure S15), and difficulty in resolving the peaks in the MS without activation, a similar plot for DMPG could not be generated here.

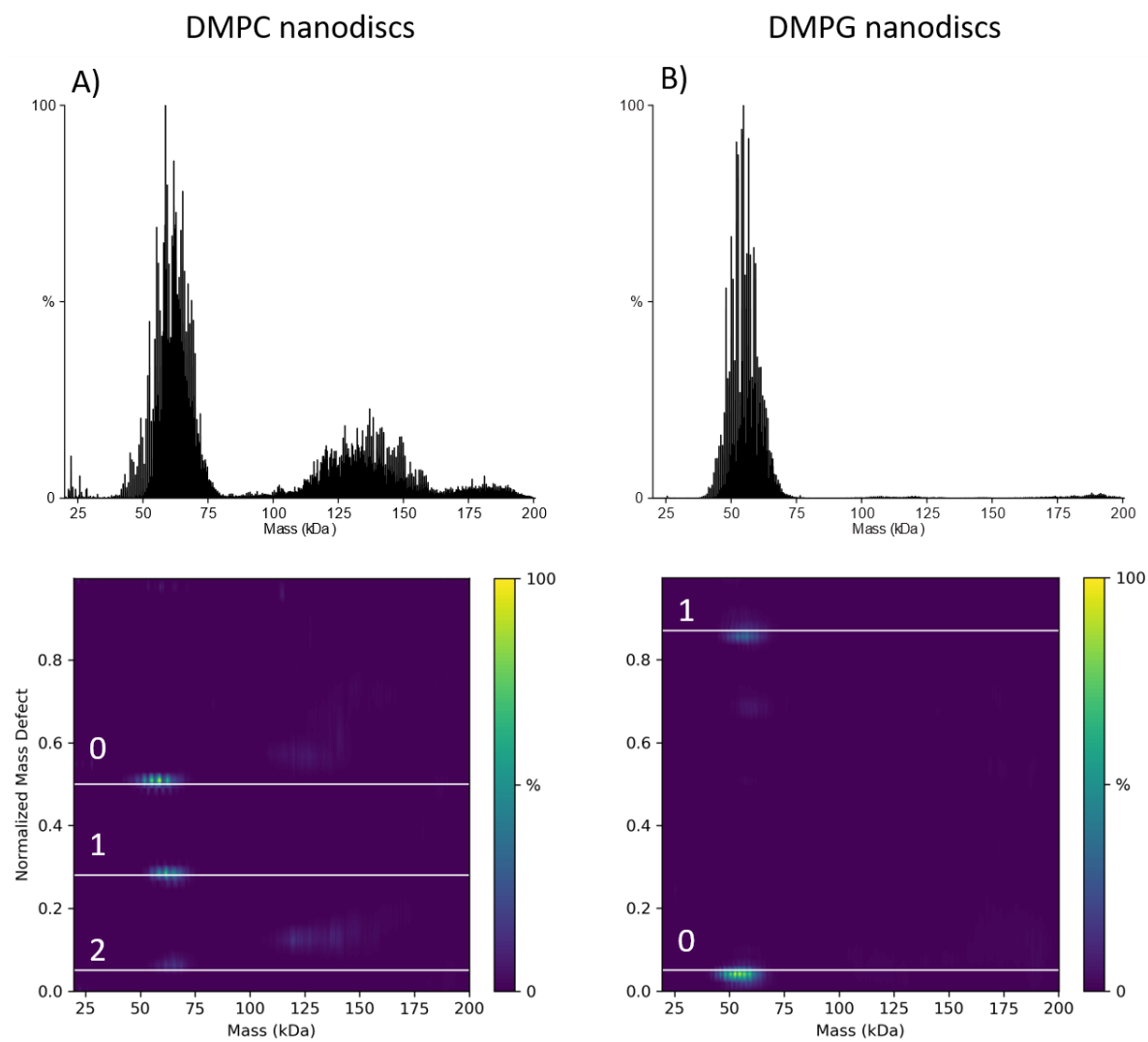


Figure S19: SID (125 V) dissociation of gramicidin-containing nanodiscs yields split nanodiscs (top, as labeled) and corresponding macromolecular mass defect plots (bottom) show that the half nanodiscs can retain gramicidin. Horizontal lines in mass defect plots represent one membrane scaffold belt protein and variable numbers of gramicidin from 0-2 and are labelled for the number of gramicidin peptides.

References

1. Reid, D. J.; Keener, J. E.; Wheeler, A. P.; Zambrano, D. E.; Diesing, J. M.; Reinhardt-Szyba, M.; Makarov, A.; Marty, M. T., Engineering nanodisc scaffold proteins for native mass spectrometry. *Analytical chemistry* **2017**, *89* (21), 11189-11192.
2. Ritchie, T.; Grinkova, Y.; Bayburt, T.; Denisov, I.; Zolnerciks, J.; Atkins, W.; Sligar, S., Reconstitution of membrane proteins in phospholipid bilayer nanodiscs. *Methods in enzymology* **2009**, *464*, 211-231.
3. Marty, M. T.; Zhang, H.; Cui, W.; Blankenship, R. E.; Gross, M. L.; Sligar, S. G., Native mass spectrometry characterization of intact nanodisc lipoprotein complexes. *Analytical chemistry* **2012**, *84* (21), 8957-8960.
4. Walker, L. R.; Marzluff, E. M.; Townsend, J. A.; Resager, W. C.; Marty, M. T., Native mass spectrometry of antimicrobial peptides in lipid nanodiscs elucidates complex assembly. *Analytical chemistry* **2019**, *91* (14), 9284-9291.
5. Marty, M. T.; Baldwin, A. J.; Marklund, E. G.; Hochberg, G. K. A.; Benesch, J. L. P.; Robinson, C. V., Bayesian deconvolution of mass and ion mobility spectra: from binary interactions to polydisperse ensembles. *Analytical chemistry* **2015**, *87* (8), 4370-4376.
6. Reid, D. J.; Diesing, J. M.; Miller, M. A.; Perry, S. M.; Wales, J. A.; Montfort, W. R.; Marty, M. T., MetaUniDec: high-throughput deconvolution of native mass spectra. *J Am Soc Mass Spectr* **2018**, *30* (1), 118-127.
7. Marty, M. T.; Hoi, K. K.; Gault, J.; Robinson, C. V., Probing the Lipid Annular Belt by Gas-Phase Dissociation of Membrane Proteins in Nanodiscs. *Angewandte Chemie International Edition* **2016**, *55* (2), 550-554.
8. VanAernum, Z. L.; Gilbert, J. D.; Belov, M. E.; Makarov, A. A.; Horning, S. R.; Wysocki, V. H., Surface-induced dissociation of noncovalent protein complexes in an extended mass range orbitrap mass spectrometer. *Analytical chemistry* **2019**, *91* (5), 3611-3618.
9. Harvey, S. R.; Seffernick, J. T.; Quintyn, R. S.; Song, Y.; Ju, Y.; Yan, J.; Sahasrabudhe, A. N.; Norris, A.; Zhou, M.; Behrman, E. J., Relative interfacial cleavage energetics of protein complexes revealed by surface collisions. *Proceedings of the National Academy of Sciences* **2019**, *116* (17), 8143-8148.
10. Silvius, J. R., Thermotropic phase transitions of pure lipids in model membranes and their modifications by membrane proteins. *Lipid-protein interactions* **1982**, *2*, 239-281.
11. Wysocki, V. H.; Jones, J. L.; Ding, J. M., Polyatomic Ion Surface Collisions at Self-Assembled Monolayer Films. *J Am Chem Soc* **1991**, *113* (23), 8969-8970.
12. Kane, T. E.; Somogyi, A.; Wysocki, V. H., Reactive Ion-Surface Collisions - Application of Ionized Acetone-D(6), DmsO-D(6) and Pyridine-D(5) as Probes for the Characterization of Self-Assembled Monolayer Films on Gold. *Org Mass Spectrom* **1993**, *28* (12), 1665-1673.